A silk composite fiber reinforced by telechelic-type polyalanine and its strengthening mechanism†

Jianming Chen,[a] Kousuke Tsuchiya,[b] Hiroyasu Masunaga,[c] Ali D. Malay[a] and Keiji Numata ![ORCID] *[a,b]

Antiparallel β-sheets play a key role in determining the physical properties of fibroins, *e.g.*, degradation and mechanical properties, and are typically formed by poly(A) motifs from spider dragline silks and GAGAGS motifs from *Bombyx mori* silkworm silks. To explore the interaction between these two motifs within the same system, a telechelic-type polyalanine (TPA) was prepared through chemoenzymatic synthesis and doped in silkworm silk fibroins to fabricate silk composite fibers. Interestingly, when TPA was added at suitable ratios of 1 and 3 wt%, the mechanical properties of the composite fibers were largely improved by approximately 42% and 51% compared with those of silk-only fibers in terms of tensile strength and toughness, respectively. As revealed by wide-angle X-ray diffraction (WAXD), silk composite fibers achieved the highest crystallinity at a TPA ratio of 1 wt%, largely contributing to their tensile strength. Evidenced by simultaneous stretching during WAXD measurement, TPA did not compete with the silk matrix by forming its own crystallization. Ultimately, a strengthening mechanism of nucleus-dependent crystallization was discussed to show the favorable heterogeneous nucleation created from TPA molecules for the promotion of crystallization in silk fibroins. Interestingly, regularly packed and aligned granules within composite fibers were detected by AFM to further support the enhanced mechanical performance. This work envisions sophisticated control of β-sheet crystals to better understand the structure–property relationship.

Introduction

Silk fibroins are unique proteins with application-oriented processing potential. Especially in the form of fibers, the desire to pursue high-performance artificial fibers regenerated from abundant silkworm silks has never faded. Despite intensive investigation of the silk assembly mechanism to inspire spinning,[1–3] two central scientific issues remain challenging for the artificial spinning process. One is how to largely retain the molecular weight. Based on the gold standard in the degumming and dissolving process,[4] it is inevitable to find certain hydrolysis and degradation of molecular chains within silk fibroins. The other is how to control the crystallization. It

is widely accepted that the phase separation from soluble proteins to solid fibers is triggered in order,[5,6] where a subtle alignment of crystals with a favorable size and orientation is considered significant for the mechanical properties of the resultant fibers. Current technical issues regarding silk crystallization make it difficult to control the crystallization rate by either an alcohol-involved organic system or aqueous spinning using pH and ionic strength gradients.[2,7]

The GAGAGS motif was realized to form a β-sheet with a dominant content of Gly and Ala within *Bombyx mori* silks.[8] However, poly(A) and poly(GA) motifs were found in *Trichonephila clavipes* dragline silks to form antiparallel β-sheets.[9] In comparison with spider dragline silks, mulberry silkworm silks possess a higher β-sheet content (~50%) but lower mechanical properties. Interestingly, nonmulberry silkworms (such as *Samia cynthia ricini* and *Antheraea pernyi*) were reported to have higher extensibility than mulberry silkworms.[10,11] Similar to dragline silks, tandem repeats of poly(A) alternated in the repetitive domains of the primary sequence in nonmulberry silkworm silks.[12] β-Sheets were thought to be finally involved in the crystalline or semicrystalline regions of silk fibers.[13]

[a]Biomacromolecules Research Team, RIKEN Center for Sustainable Resource Science, 2-1 Hirosawa, Wako, Saitama 351-0198, Japan

[b]Department of Material Chemistry, Kyoto University, Nishikyo-ku, Kyoto 615-8510, Japan. E-mail: numata.keiji.3n@kyoto-u.ac.jp

[c]Japan Synchrotron Radiation Research Institute, 1-1-1, Kouto, Sayo-cho, Sayo-gun, Hyogo 679-5198, Japan

†Electronic supplementary information (ESI) available. See DOI: 10.1039/d2py00030j

To improve the mechanical properties, natural rubber (NR),[14] collagen,[15] hydroxyapatite (HA),[16,17] poly(lactic acid) (PLA)[18] and graphene[19] were added to silk fibroins for biomedical applications. Although these additives are usually biocompatible or biodegradable to meet various application requirements, the problem of building strong interfacial cohesion between silk fibroins and additives remains largely unsolved. Furthermore, in-depth investigations have rarely been reported to analyze the mechanism for the improved mechanical performance. It is crucial to reveal the structure–property relationship on a molecular scale to clearly understand the effect of additives on the silk crystalline structure, namely, the orientation and amounts of β-sheet crystals.

Polyalanine is expected to be one of the best candidates to strengthen silk fibroins when its miscibility and abundance within spider and silkworm silks are taken into consideration. As reported earlier,[20] genetic engineering was conducted to introduce more poly(A) motifs from *Latrodectus hesperus* MaSp1 to transgenic vectors of silkworms, enabling the fracture strength and modulus to be enhanced as a result of increased β-sheet contents. In our previous studies,[21,22] a telechelic polyalanine (designated TPA) was fabricated that showed better solubility in various solvents (such as HFIP and methanol solution) than linear polyalanine with similar chain lengths. In addition, TPA was able to self-assemble into nanofibrils. The interaction between TPA and silk fibroins was discussed to illustrate the improved mechanical properties of silk composite films. In this work, TPA was introduced into silk fibroins for the preparation of silk composite fibers. From the viewpoint of composite science, TPA can be theoretically added as a dopant in all silk morphologies, such as fibers, films, hydrogels, foams, and spheres. However, unlike conventional fillers with stable physical and chemical properties, TPA may change its secondary structure and form crystals under external stimuli, such as solvent, heat, pH and stress. From a biomimetic perspective, to better understand the role of TPA in the mechanical properties within natural spider silk, it is of significant importance to investigate TPA in fiber systems. Evidenced by the synchrotron radiation WAXD result, TPA did not independently form nanocrystals within the composite but served as a heterogeneous nucleus to facilitate the crystallization of the silk matrix, leading to enhanced mechanical properties. This molecular strengthening mechanism is totally distinct from the case of the silk composite film. Impressively, remarkable improvements of mechanical behaviors were achieved for the composite fiber in terms of stress and toughness, *i.e.*, more than 40% higher than the silk-only fiber.

Experimental section

Preparation of silk fibroins

Similar to the previously reported method,[23] silk fibroins were prepared from *B. mori* silkworm cocoons. Specifically, cocoons were cut into pieces and then boiled in 0.02 M Na_2CO_3 solution for 30 min to remove the sericin. After thoroughly washing with Milli-Q water three times, degummed silks, designated De-silk, were completely dried in a fume hood. Subsequently, De-silk were dissolved in 9.3 M LiBr (Sigma Aldrich) solution at 60 °C for 40 min under continuous stirring. The obtained silk solution was dialyzed against Milli-Q water by using SnakeSkin tubing (MWCO: 3.5 kDa, 22 mm ID, Thermo Fisher) for three days and then centrifuged to remove impurities. Finally, the silk fibroins were lyophilized and stored at −80 °C prior to use.

Synthesis of bis(alanine ethyl ester) initiator (1)

Alanine ethyl ester hydrochloride (4.76 g, 31 mmol), triethylamine (9.2 mL, 66 mmol), and ethyl acetate (100 mL) were added to a 200 mL flask equipped with a stir bar and an addition funnel. To this mixture, a solution of succinyl chloride (1.7 mL, 15 mmol) in ethyl acetate (50 mL) was added dropwise at 0 °C under nitrogen. The resulting solution was stirred at 0 °C for 2 h, and the reaction was quenched by the addition of water. The mixture was washed with water, sodium bicarbonate aq. (1 M), and brine. The organic layer was dried with sodium sulfate and concentrated using a rotary evaporator. The crude product was recrystallized from hexane/ethyl acetate to afford a pale-yellow, needle-shaped crystal. The yield was 3.84 g (78%).

Synthesis of TPA by chemoenzymatic polymerization

TPA was synthesized by chemoenzymatic polymerization.[24] To a round bottom flask equipped with a stir bar, alanine ethyl ester hydrochloride (6.45 g, 42 mmol), 1 (3.84 g, 12.1 mmol), phosphate buffer (14 mL, 1 M, pH 8.0), and methanol (7.0 mL) were added, and the mixture was stirred at 40 °C until all substrates were completely dissolved. Then, a solution of papain (2.10 g) in phosphate buffer (14 mL) was added in one portion. The final concentrations of alanine ethyl ester and papain were 1 M and 50 mg mL^{-1}, respectively. The mixture was stirred at 40 °C and 800 rpm for 6 h. After cooling to room temperature, the precipitate was collected by centrifugation at 9000 rpm and 4 °C for 15 min. The crude product was washed twice with deionized water and methanol and lyophilized to afford a white powder. The yield was 1.05 g. Linear polyalanine (LPA) was also synthesized by using a similar method without initiator **1**.[25,26]

Fabrication of silk composite fibers

Silk composite fibers were fabricated by adding TPA to silk fibroins at different ratios ranging from 0.5 to 5 wt%. The typical procedure to make silk fibers with 1 wt% TPA, designated Silk/TPA-1, is described here. Lyophilized silk fibroins (300 mg) and TPA (3 mg, 1 wt% to the silk fibroin) were completely dissolved in 1,1,1,3,3,3-hexafluoro-2-propanol (HFIP, 1.4 mL) to form a spinning dope with a concentration of 18 w/v%. To avoid aggregation or poor dispersion, TPA was first dissolved in HFIP under stirring for 3 h, and then silk fibroins were added for dissolution in another 3 h to finally obtain the transparent dope. Then, the silk dope was transferred to a syringe (spinneret ID: 0.25 mm) for wet spinning, where the

syringe pump was equipped with a coagulation bath containing 90% isopropanol (IPA) solution. For posttreatment, a single pristine silk fiber was first immersed in 80% ethanol for 1 min and then manually stretched to 300% of its initial length with a final average diameter of 78 μm. To induce more crystals, poststretched fibers were put in 90% methanol for 1 h. Silk fibers with other TPA ratios (0.5, 3 and 5 wt%) were fabricated using the same method and designated Silk/TPA-0.5, Silk/TPA-3 and Silk/TPA-5. For comparison, silk-only fiber was directly prepared from silk fibroins without the addition of TPA. Notably, the Silk/TPA-5 fiber can only be poststretched to a maximum of 200%.

Synchrotron radiation X-ray diffraction

The crystallization and orientation of silk fibers were investigated by synchrotron-radiation WAXD at Spring-8, Harima. The BL05XU beamline was used with an X-ray energy of 12.4 keV and a wavelength of 0.1 nm. The sample-to-detector distance was 267 mm, and the exposure time for each sample was 1 s. 1D profiles were converted from 2D patterns by using Fit2D software.[27] After peak fitting with a Gaussian function, the crystallinity (χ_c) can be estimated by the following equation:

$$\chi_c = \frac{A_c}{A_c + A_a} \times 100\% \tag{1}$$

where A_c and A_a are the integrated areas of crystalline and amorphous peaks, respectively.

The crystallite size (D) at the (020) reflection can be calculated according to the Scherrer equation:

$$D = \frac{k\lambda}{\beta \cos \theta} \tag{2}$$

where D is the crystallite size, K is the shape factor, λ is the wavelength of the X-ray beam, β is the full width at half-maximum (FWHM) of the peak, and θ is the Bragg angle. Here, K is taken as a value of 0.9 according to a previous study.[28]

The degree of orientation (χ_o) at the (020) reflection was calculated by:

$$\chi_o = \frac{180 - \beta_1}{180} \times 100\% \tag{3}$$

where β_1 is the FWHM (azimuthal angle) at the (020) reflection.

Simultaneous stretching of silk composite fibers (with a TPA ratio of 0.5, 1 and 3 wt%) was carried out during the WAXD measurement. A bundle of fibers was well aligned to the stretching direction and fixed on a load cell (20 N). Tensile deformation was performed using a custom-made uniaxial tensile testing machine at 25.5 °C, 48% RH, and a strain rate of 2 mm min⁻¹. The signal was collected in 1 s with a 5 s interval until the sample fractured.

Analytical methods

The ¹H NMR spectrum was collected on a Varian NMR System 500 (Palo Alto, CA) at 25 °C with a frequency of 500 MHz. Dimethylsulfoxide-d_6 (DMSO-d_6) and trifluoroacetic acid-d (TFA-d) were used in a volume of 5/1 to dissolve the TPA with

tetramethylsilane (TMS) as the internal standard. CD measurements were conducted in a JASCO J-820 spectropolarimeter at 25 °C. The samples were dissolved in HFIP to a concentration of 0.2 mg mL⁻¹ and transferred to a quartz cuvette with a path length of 0.1 cm. CD spectra were recorded over five scans at a scanning speed of 50 nm min⁻¹, a bandwidth of 1 nm and a data pitch of 0.1 nm. SEM measurements were conducted by fixing fiber samples using conductive carbon tape onto an aluminum stub. After gold sputtering (Smart Coater, JEOL) for 2 min, the surface morphology of the samples could be well visualized using a JEOL-6000 instrument at an acceleration voltage of 15 kV under high vacuum. To obtain the cross section, the fiber sample was first immersed in liquid nitrogen for 1 min and then cut with a blade. Raman spectra were recorded using JASCO NRS-4100 equipment with a laser beam excited at 532 nm. Silk fibers or polyalanine powders were sandwiched between the glass slide and cover slip before applying a 100× oil objective lens. Spectra were recorded ranging from 500 to 2000 cm⁻¹ under a grating of 900 grooves per mm and a slit size of 50 × 8000 μm. Consistent results were obtained by using a beam intensity of 16.9 mW, an exposure time of 10 s and an accumulation of three times. All spectra were finally normalized by the internal standard peak at 1450 cm⁻¹. The secondary structure of silk fibers and TPA can be determined by ATR-FTIR (IRPrestige-21, Shimadzu). A Ge prism was used as the MIRacle A single-reflection ATR unit. Different from the TPA powders, a bundle of silk fibers was chopped into small pieces before measurement. The wavenumber ranged from 650 to 4500 cm⁻¹ at a resolution of 4 cm⁻¹, while the spectra were averaged over 8 scans with the apodization function of Happ-Genzel. The spectra were normalized for deconvolution within the amide I region from 1580 to 1720 cm⁻¹. A tensile test was performed on a mechanical testing machine (EZ-LX/TRAPEZIUM X, Shimadzu) at 23 °C and 35–50% RH. Silk fibers were mounted on a cardstock with a 20 mm distance between jigs. The average diameter of the samples was determined by optical microscopy. A 50 N loading cell was used for the silk-only and composite fibers with a strain rate of 10 mm min⁻¹. To improve the accuracy, a 1 N loading cell was chosen for native cocoon silk and De-silk. The testing number for each sample was 8. Tukey's honest significant difference (HSD) was combined with one-way ANOVA to analyze the results using IBM SPSS Statistics.

Results and discussion

Preparation of silk composite fibers containing TPA

The synthesis of TPA was conducted by chemoenzymatic polymerization by using papain as previously reported.[29] The structure of TPA was confirmed by ¹H NMR spectroscopy (Fig. S1, ESI†) with an average molecular weight (M_n) of 800. For comparison, LPA (M_n = 700) was synthesized under conditions similar to TPA, and their chemical structures are illustrated in Fig. 1a. Because LPA has a strong tendency to form β-sheets *via* hydrogen bonds, it can hardly dissolve in HFIP,
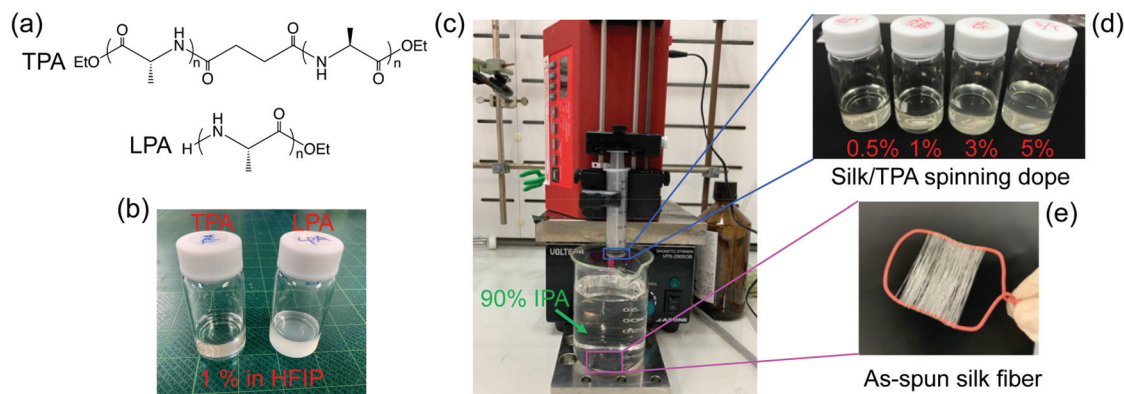
Fig. 1 The preparation of silk composite fibers by the addition of TPA. (a) Chemical structures of TPA and LPA; (b) the appearance of (1 wt/v %) TPA and LPA in HFIP; (c) wet spinning setup through a syringe pump with a 90% IPA solution as the coagulator; (d) the appearance of the silk/TPA spinning dope at ratios from 0.5 to 5 wt%; (e) as-spun silk fibers collected from the coagulation bath.

finally forming an opaque suspension (Fig. 1b). However, in the case of TPA, a transparent solution was observed after complete dissolution in HFIP. Although a series of spinning methods have been developed in recent years to fabricate artificial silk fibers, wet spinning equipped with an alcoholic coagulation bath is still popular due to the ease of use. Here, a syringe pump was applied to control the feed speed of silk dopes, and 90% IPA was used as the coagulator (Fig. 1c). As expected, large aggregates were visualized when mixing LPA with silk fibroins in HFIP (Fig. S2, ESI†). Therefore, LPA is not suitable as a dopant for silk composite fibers. In contrast, TPA could be homogeneously dispersed in the silk solution in a ratio of up to 5 wt% (Fig. 1d), demonstrating good miscibility with the silk matrix. After spinning at a dope concentration of 18 w/v%, silk composite fibers were collected and mounted on a steel frame (Fig. 1e). As a control, silk-only fiber was prepared under the same spinning conditions.

To make robust fibers, pristine silk fibers were post-stretched and immersed in methanol for higher crystallization. The surface morphology of posttreated fibers could be determined by SEM. As shown in Fig. 2, a groove-like structure was clearly developed along the fiber axis, which may be induced by the shearing force generated along the wall of the syringe during the spinning process. It is worth noting that unevenness in the diameter (Fig. 2e) was only observed for Silk/TPA-5 fibers, probably due to the aggregation of excessive TPA. This result explained why pristine Silk/TPA-5 fibers could only be poststretched to a maximum of 200%, while other fibers could achieve 300%. The cross section was dense and free of visible defects for both silk-only and composite fibers (Fig. 2f–j).

Secondary structures of Silk/TPA composites

The secondary structure of silk-only, TPA and silk composites in HFIP can be determined by CD spectra. As shown in Fig. 3, pure TPA mainly adopted a random coil structure with the typical negative ellipticity at 195 nm. This result was in good agreement with some peptides, such as $(AG)_{15}$, but different from others such as $(AGSGAG)_5$.[30] It is assumed that the polar hydroxy groups of serine residues would interact with HFIP molecules to stabilize the formation of helical structures. Perceptibly, distinct CD results were found for silk-only and silk composite solutions with the primary conformation of the α-helix, which was reflected by the negative peaks at 204 and 220 nm. As previously reported,[31] silk fibroins may adopt
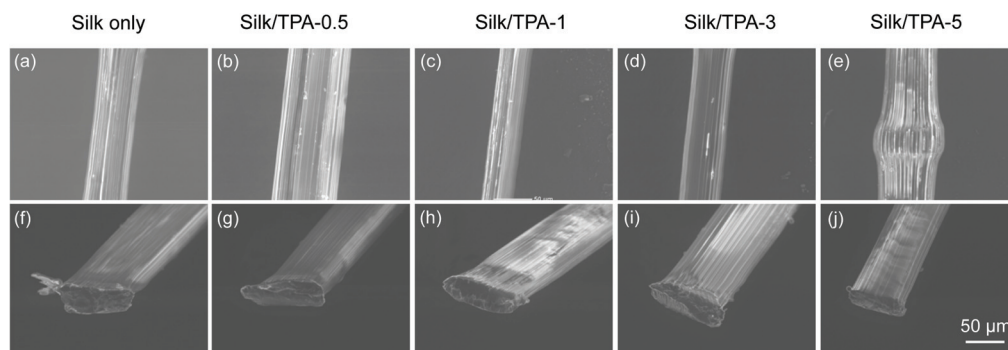

Fig. 2 SEM images of silk-only fiber (a and f), Silk/TPA-0.5 fiber (b and g), Silk/TPA-1 fiber (c and h), Silk/TPA-3 fiber (d and i) and Silk/TPA-5 fiber (e and j) after posttreatment. Fibers were transferred to liquid nitrogen and then cut with a blade to obtain cross-sections.
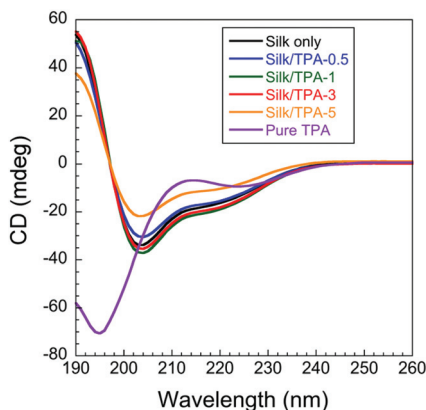
Fig. 3 CD spectra of pure silk, pure TPA and silk/TPA composites in HFIP.

various secondary structures when dissolved in water or in HFIP. Similar to silkworm silk fibroins, different types of spider silk proteins adopted the same secondary structure in HFIP.[32,33] The polar HFIP molecules enabled silk fibroin molecules to favorably fold into helical structures. Overall, the addition of TPA to the silk matrix does not alter the conformation of silk fibroins. In other words, there is no obvious interaction between TPA and silk fibroins in the solution.

The change in secondary structures from pristine to posttreated fibers was investigated by Raman spectroscopy. Fig. 4a shows a difference in the Raman shift between LPA and TPA. The β-sheet-rich structure of LPA was indicated by the typical three peaks at 1665, 1234 and 1086 cm^{-1}, which were assigned to C=O stretching in the amide I region, CH$_2$ twisting in the amide III region and C–C skeletal stretching, respectively.[34,35] When compared with LPA, TPA has a relatively lower β-sheet content according to a blueshift from 1665 to 1661 cm^{-1} and a redshift from 1086 to 1095 cm^{-1}.

As suggested by CD, soluble silk-only and composite solutions primarily obtained helical structures. However, after spinning into the corresponding solid fibers, more β-sheets were induced by IPA within the coagulation bath, as confirmed by Raman spectra (Fig. 4b). After normalization at the standard internal peak of 1450 cm^{-1}, a substantial increase in
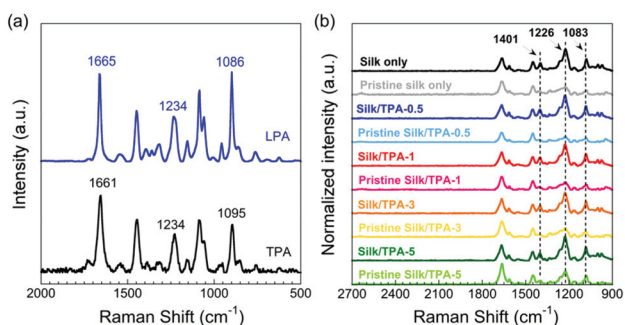
intensity was presented at peaks 1401, 1226 and 1083 cm^{-1} after posttreatment of pristine silk fibers. The poststretching and further methanol treatment facilitated the formation of more β-sheets, resulting in the enhancement of the intensity at 1226 and 1083 cm^{-1}. Intriguingly, the peak at 1401 cm^{-1} was assigned to H bending in poly(A) or CH$_2$ wagging in poly(AG),[26] indicating increased β-sheets constituted by poly(A) from TPA and/or by poly(AG) from silk fibroins.

To be more specific, semiquantitative analysis was conducted for the related three peaks (Fig. 5). Silk composite fibers shared a similar tendency of intensity change at peaks 1226 and 1083 cm^{-1} in the Raman spectra (Fig. 5a and b). Before posttreatment, the peak intensity of silk composite fibers gradually increased with increasing TPA ratio from 0.5 to 5 wt%. In contrast, at the 1401 cm^{-1} peak, the overall result was reflected by the competition between poly(A) from TPA and poly(AG) from silk fibroins (Fig. 5c). After posttreatment, the peak intensity of silk composite fibers was higher than that of silk-only fibers at the three relevant peaks. According to the change ratio of intensity for the three peaks shown in Fig. 5d, the posttreatment had the most profound effect on the Silk/TPA-0.5 fibers. Intriguingly, adding suitable amounts of TPA from 0.5 to 3 wt% to the silk matrix may be favorable for the promotion of poly (AG)-involved β-sheet formation.

In addition to Raman spectroscopy analysis, the secondary structure of silk fibers was further verified by ATR-FTIR spectroscopy. The absorbance of the samples was normalized within the amide I region from 1710 to 1590 cm^{-1} (Fig. 6a),
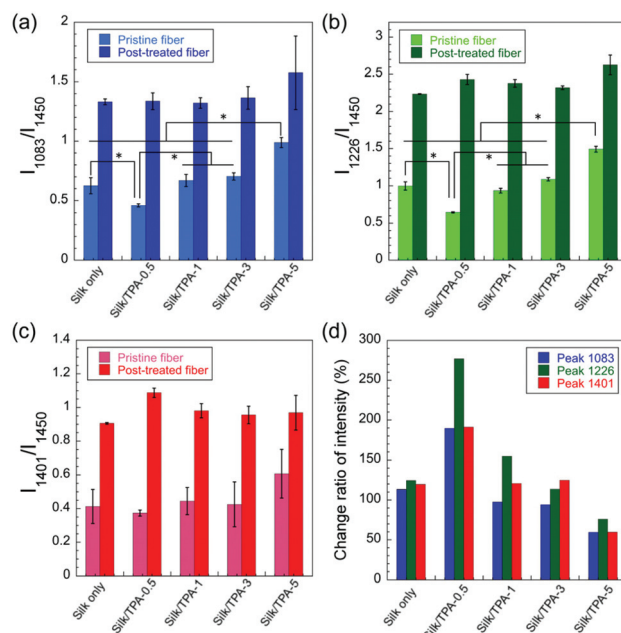

Fig. 5 The relative intensity of pristine and posttreated fibers at peaks (a) 1083 cm^{-1}, (b) 1226 cm^{-1} and (c) 1401 cm^{-1} against the internal standard peak at 1450 cm^{-1} in the Raman spectra in Fig. 4. (d) The change ratio of intensity at the three related peaks. The change ratio of intensity was defined as the posttreatment intensity divided by the pristine intensity.
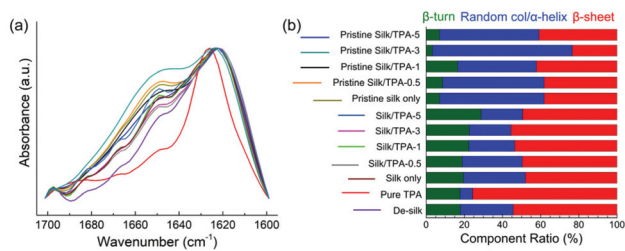

Fig. 4 Raman spectra of (a) polyalanine powders and (b) silk fibers before and after posttreatment.

Paper

Polymer Chemistry

Fig. 6 ATR-FTIR absorbance of (a) silk fibers within the amide I region and the related (b) component ratio of secondary structures after deconvolution.

and the related deconvolution was carried out to calculate each component ratio (Fig. S3, ESI†). As shown in Fig. 6b, pure TPA comprised more than 70% β-sheets. De-silk was detected with nearly 54% β-sheets, which was comparable to the content previously reported on similar degummed fibers from *B. mori* silkworm silks.[36] In line with the Raman result, the β-sheet of silk fibers was increased after posttreatment.

Mechanical properties of silk composite fibers

In addition to the investigation of secondary structures, the influence of TPA, as a dopant, on the mechanical properties was also evaluated to exhibit a representative stress–strain curve (Fig. 7a). As clearly depicted in Fig. 7b, all silk composite fibers achieved significantly higher yield stress than silk only fibers, rendering composite fibers promising materials for

high-performance applications. For TPA added at 0.5 wt%, the tensile strength of the Silk/TPA-0.5 fiber was not significantly different from that of the silk-only fiber (Fig. 7c). However, remarkably improved strength was obtained by increasing the TPA ratios to 1 and 3 wt%. Impressively, the highest tensile strength of 250 MPa was achieved for the Silk/TPA-1 fiber, which was approximately 42% higher than that of the silk-only fibers. Notably, the tensile strength of the Silk/TPA-5 fibers was even lower than that of the silk-only fibers. The main reason may be the aggregation of excessive TPA inside the silk matrix causing stress concentration. The special knot structure in SEM could also explain the adverse mechanical behavior. The elastic modulus of bulk silk fibers was closely associated with the β-sheet, including its size, orientation and content. For most composites, the modulus can be improved by reinforced fillers. In this work, TPA might also increase the modulus of composite fibers but there was no statistically significant difference between silk only and composite fibers (Fig. 7d). Interestingly, the highest toughness of 44 MJ cm^{-3} was obtained for the Silk/TPA-3 fibers, approximately 51% higher than the silk-only fibers (Fig. 7e). Both the high tensile strength and extensibility (Fig. 7f) contributed to the ultimate toughness of the Silk/TPA-3 fibers. The silk composite fibers were compared with native cocoon silks and De-silk regarding the mechanical properties (Fig. S4 and S5, ESI†). In comparison with native cocoon silks, Silk/TPA-1 fibers exhibited a higher stress, while Silk/TPA-3 fibers exhibited both higher strain and toughness. However, De-silk still exhibited higher stress and modulus than these two composite fibers. One
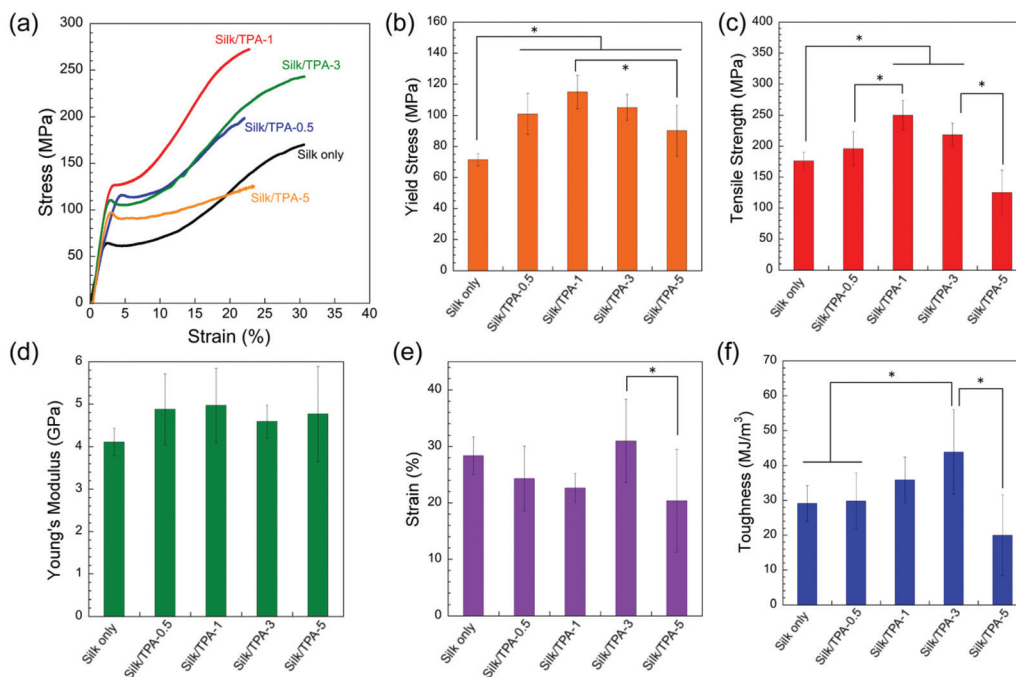

Fig. 7 Representative stress–strain curves of (a) silk-only and silk composite fibers with detailed mechanical properties in terms of (b) yield stress, (c) tensile strength, (d) Young's modulus, (e) strain and (f) toughness. * Significant difference between groups at $p < 0.05$. The testing number for each sample is eight.

main reason should be the difference in the molecular weight. Another reason could be deduced from the cross-sectional structure of fiber samples after tensile testing (Fig. S6 and S7, ESI†). De-silk possessed a denser structure than silk-only and composite fibers, partly attributed to the distinct fiber spinning process.

Crystalline structure of silk composite fibers using WAXD analysis

Synchrotron-radiation WAXD measurements (Fig. S8, ESI†) were conducted to elucidate the interaction between TPA and silk fibroins and the effect of TPA on the crystallization behavior of the silk matrix. 1D WAXD profiles of silk-only and composite fibers are presented in Fig. 8a. De-silk and pure TPA were also included for comparison. De-silk showed an antiparallel β-sheet with two major peaks at 0.45 and 0.37 nm, which were assigned to the Miller indices of (020) and (021), respectively.[37]

For TPA, three main peaks with d-spacings of 0.52, 0.43 and 0.37 nm demonstrated the formation of β-sheets by polyalanine sequences.[38,39] After posttreatment, the intensity of silk fibers was largely increased, especially at peaks (010), (210) and (022), when compared with pristine silk fibers (Fig. S9a, ESI†). It is worth noting that no obvious characteristic peaks from the β-sheet of TPA were observed for silk composite fibers before and after posttreatment. This result was different from the TPA-doped silk composite films reported in our previous studies,[17,18] where TPA and silk fibroins could independently form their own β-sheet crystals. The major reason behind the difference may be the distinct strengthening mechanisms in the form of the film and fiber. Although the mechanical properties of silk composite films were improved compared to silk-only films, a more significant mechanical enhancement was obtained in the case of silk composite fibers. We assumed that TPA was actively involved in the crystallization of silk fibroins and functioned like a heterogeneous nucleus.

The azimuthal intensity at the radially integrated peak (020) is shown in Fig. 8b, and the degree of orientation can be calculated based on the FWHM. A smaller FWHM means a higher orientation degree. Obviously, after posttreatment, silk fibers obtained a much higher degree of orientation than pristine fibers (Fig. S9b, ESI†). This result can also be roughly deduced from the interference fringes on the 2D patterns.

The degree of crystallinity can be calculated after peak fitting from 1D WAXD profiles.[40] As shown in Fig. S9c,† the crystallinity of pristine silk composite fibers shared a similar tendency, as shown in the FTIR results, with regard to the increase in TPA ratios. In other words, the crystallinity is positively related to the content of β-sheets. It seems that 1 wt% is a suitable amount using TPA to improve the crystallinity of composite fibers. After posttreatment, the crystallinity was further increased for all silk fibers and reached the highest value of ~30% for the Silk/TPA-1 fiber (Fig. 8c), which explained its impressive mechanical properties in terms of
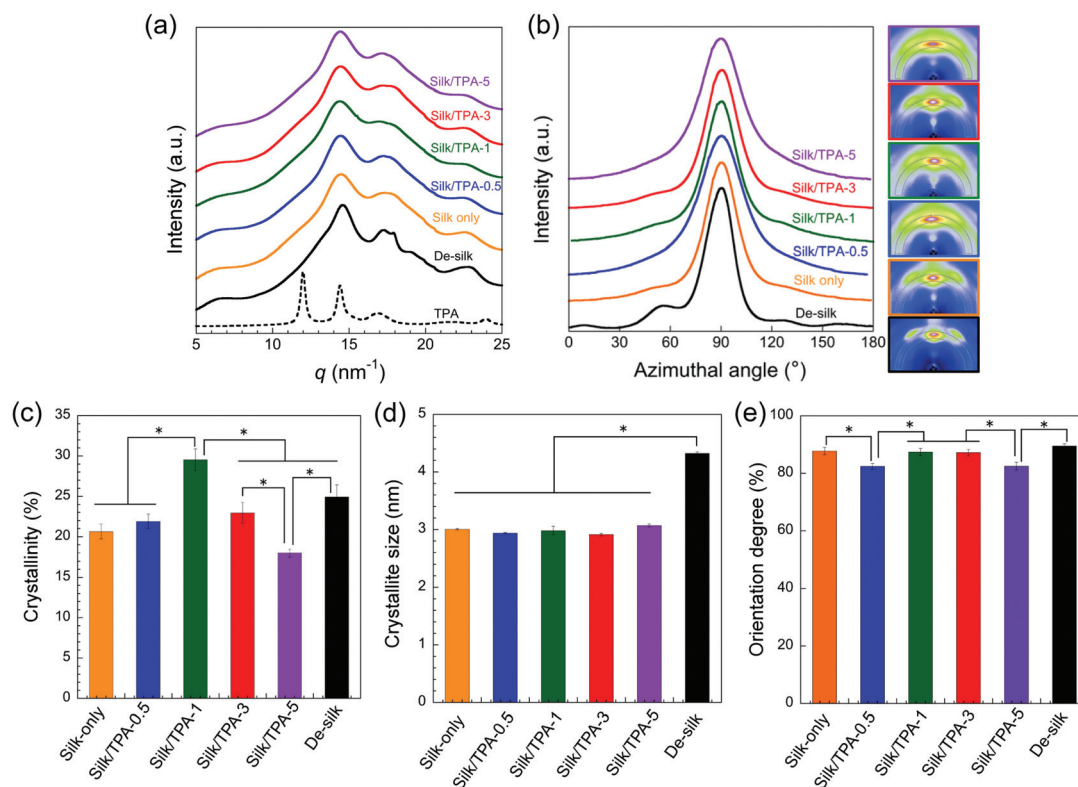

Fig. 8 Structure analysis of silk fibers by WAXD. (a) 1D integrated profiles from the 2D patterns. (b) Azimuthal intensity profile at the (020) peak. The arc lines in the 2D patterns were shown to obtain the relevant azimuthal intensity. (c) Crystallinity. (d) Crystallite size. (e) Orientation degree. * Significant difference between groups at $p < 0.05$.

stress. Raman, FTIR and solid-state NMR spectroscopy were primarily used to characterize the secondary structure of silk fibroins.[9,36,41] The β-sheet content can be calculated by deconvolution from the Amide I region in Raman and FTIR spectroscopy while from Ala Cβ peaks in ^{13}C solid-state NMR spectroscopy. The deconvolution method may vary among individuals and changes from case to case. WAXD was widely employed to estimate the crystallinity from azimuthal integration profiles. However, a big variation was found in various methods (*e.g.* integrated areas or intensities) to calculate the crystalline and amorphous components.[12] Even though, the value of crystallinity obtained from WAXD was usually lower than that of β-sheet contents calculated from the abovementioned spectroscopy. The reason behind this could probably be explained by a recent study,[42] where the β-conformations deconvolved from FTIR consisted of both β-sheets and β-crystallites. In this context, we can better understand some difference as demonstrated in Raman, FTIR and WAXD results. It is still sufficient to gain an insight into the tendency on the relative change of the β-sheet content and crystallinity at various TPA ratios.

According to the Scherrer equation,[28] the crystallite size of silk fibers was evaluated using the FWHM of the (020) reflection, which was fitted from WAXD profiles (Fig. S10 and S11, ESI†). There was no significant difference in the crystallite size between silk-only and composite fibers, but both of them were lower than those of De-silk (~4.3 nm). After posttreatment, the crystallite size (3.3 nm, Fig. S9d, ESI†) was decreased to 2.9 nm (Fig. 8d), which was in line with the literature.[33] According to

the definition of the orientation degree, 100% and 0% refer to the β-sheet aligned parallel along the fiber axis and cross section, respectively. As illustrated in Fig. S9e,† the orientation degree of all pristine silk fibers was significantly lower than that of De-silk. When TPA was added to the silk matrix, the orientation degree of nanocrystals was hindered probably due to the competition between homogeneous and heterogeneous nucleation. After post-stretching, the orientation degree was largely increased predominantly because of better alignment of molecular chains along the fiber axis. With excessive TPA, Silk/TPA-5 fiber could only be poststretched to maximum 200% so that it obtained a relatively lower orientation degree than other silk fibers with a 300% stretching ratio (Fig. 8e).

Simultaneous stretching deformation during WAXD measurement

To further investigate the structure–property relationship, the tensile deformation of silk composite fibers was performed in combination with WAXD measurements. A bundle of fibers was first aligned and fixed on a tensile testing machine, which was then transferred to the synchrotron radiation facility for X-ray scattering in the course of fiber stretching (Fig. S12, and Video S1, ESI†). The time-course WAXD data were collected at 1 s with 5 s intervals. The mechanical properties of fiber bundles (Fig. S13, ESI†) were different from that of a single fiber shown in Fig. 7, and only consecutive data were selected for plotting due to the breakage of some single fibers within the bundle. Corresponding to the stress–strain curve in Fig. 9a, the 1D profiles of Silk/TPA-1 fibers (Fig. 9b) were demonstrated
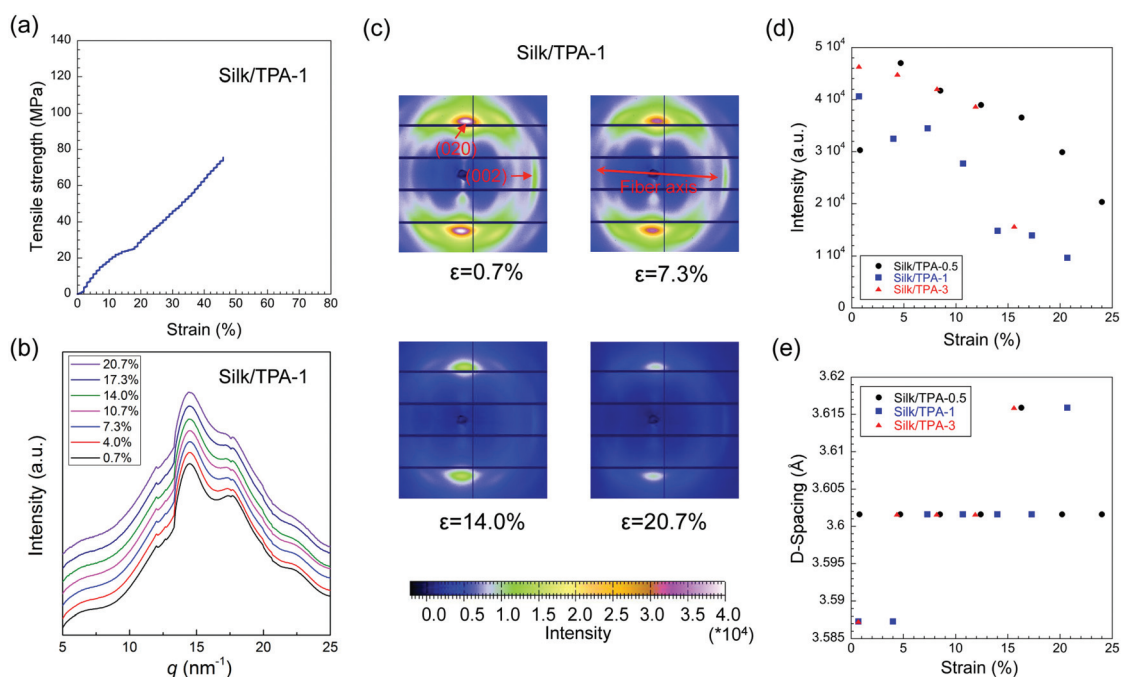

Fig. 9 Simultaneous stretching of composite fibers during WAXD measurement. (a) The stress−strain curve of Silk/TPA-1 fibers. (b) 1D profiles of WAXD results at specific strains. (c) 2D patterns showing the crystalline intensity of Silk/TPA-1 fibers at strains from 0.7% to 20.7%. The (020) and (002) reflections were perpendicular and parallel to the fiber axis, respectively. (d) The change in crystalline intensity at the (020) reflection during tensile deformation. (e) The change in *d*-spacing at the (002) reflection during fiber stretching.

at specific strains from 0.7% to 20.7%, which could be calculated from the strain rate and time intervals. In line with the result in Fig. 8, there were no new peaks, especially those coming from TPA, which appeared during the stretching process. This result suggested that TPA never formed crystallization by itself in this composite system during fiber formation, posttreatment, and tensile deformation. Here, it further proved that TPA functioned as a heterogeneous nucleate agent to facilitate the crystallization of the silk matrix. As shown in Fig. 9c, the intensity of crystallization for Silk/TPA-1 fibers gradually decreased with increasing strain. The major (020) reflection was taken to evaluate the change in crystalline intensity accompanied by fiber stretching (Fig. 9d). As the strain increased, the crystalline intensity decreased for both the Silk/TPA-1 and Silk/TPA-3 fibers, whereas it increased initially and then decreased in the case of the Silk/TPA-0.5 fibers. As previously reported,[43] dragline silks will increase crystallinity during stretching, but silkworm silks will not further crystallize. One reason may be the difference in intrinsic crystallinity between dragline and silkworm silks. It was assumed that strain-induced crystallization occurred in Silk/TPA-0.5 fibers, which obtained relatively lower crystallinity (Fig. 8c) than Silk/TPA-1 and Silk/TPA-3 fibers. The decrease in the crystalline intensity could be due to the decrease in the volume of fiber bundles as a result of tensile deformation. The (002) reflection, indicating the chain direction of β-sheet crystals parallel to the fiber axis, was found with an increased d-spacing during fiber stretching.[44]

Upon exposure to an external load, the amorphous region will be first elongated along the fiber axis. Subsequently, the crystalline region will also deform. In Fig. 9e, the tendency of the d-spacing change was similar for the Silk/TPA-1 and Silk/TPA-3 fibers. However, no obvious change in d-spacing was visualized for the Silk/TPA-0.5 fibers. The reason behind this might be that the amorphous regions within Silk/TPA-0.5 fibers accounted for most of the elongation within this range of strain.

Nano- and submicron-structures of TPA and fibers

SEM has already been applied to elucidate the morphology of silk fibers; here, AFM was further used to detect subtle details at the submicron and nanoscale. As shown in Fig. 10a, irregular particles formed after direct evaporation of HFIP from the TPA solution (Fig. S14a, ESI†). Interestingly, the self-assembly of nanofibrils (Fig. 10b and Fig. S14b, ESI†) can be induced by adding the TPA solution to IPA, which was analogous to our previous study.[18] As studied previously, nanoscale granules could be observed from natural silks[45,46] or alcohol-treated silk fibroins.[47] Similarly, for silk-only fiber, uniform granules were detected, and each of them linked together to form a pearl-like strand, aligning toward the fiber axis (Fig. 10c). By the addition of 0.5 wt% TPA, the granular structure was partly destroyed (Fig. 10d). This result could be attributed to the altered nucleating or crystalline behaviors of the silk matrix after the introduction of TPA additives. It is interesting to find a higher-order structure in the Silk/TPA-1 and Silk/TPA-3 fibers (Fig. 10e and f), where each single granule was tightly stacked in order. This higher-order structure also contributes to the enhanced mechanical performance. Evidenced by WAXD (Fig. 8e) and AFM (Fig. 10c–f), a similar result was revealed to show the lower orientation of nanocrystals and granules in Silk/TPA-0.5
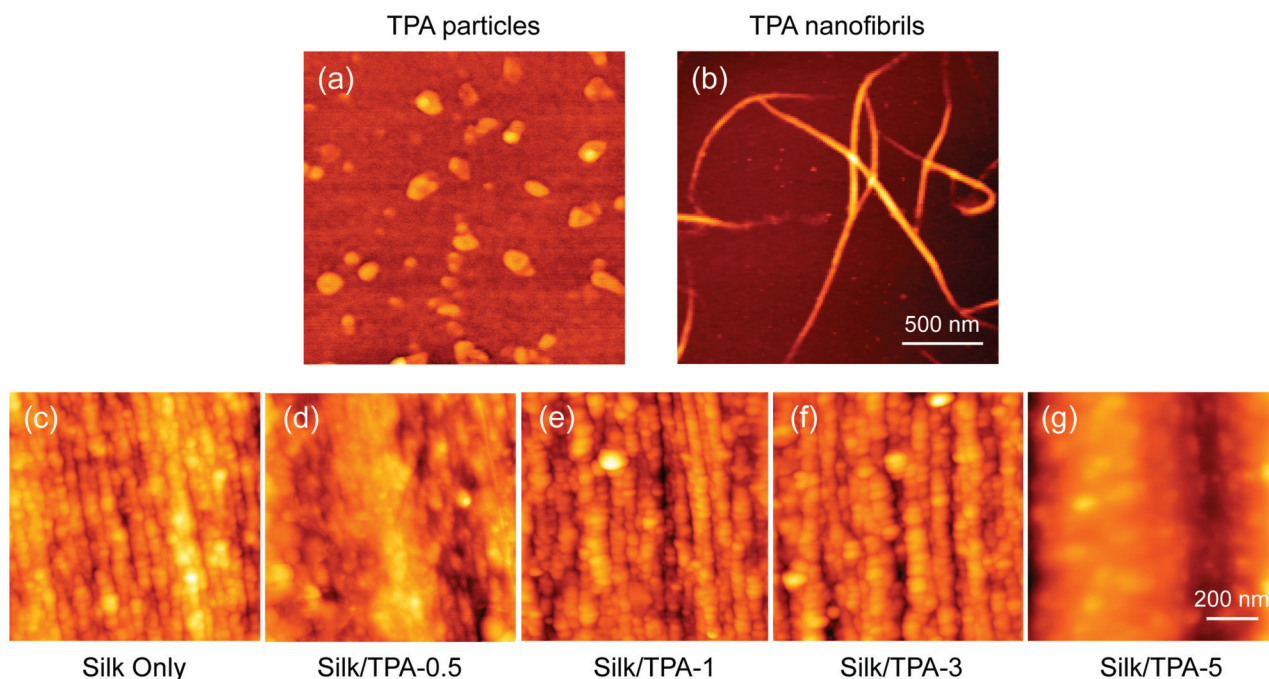

Fig. 10 AFM images of TPA and silk fibers. TPA (a) particles and (b) nanofibrils prepared without and with isopropanol, respectively. The morphology and granule distribution of (c) silk-only fiber, (d) Silk/TPA-0.5 fiber, (e) Silk/TPA-1 fiber, (f) Silk/TPA-3 fiber and (g) Silk/TPA-5 fiber.

fiber when compared with silk only, Silk/TPA-1 and Silk/TPA-3 fiber. Notably, when excessive TPA was added, such as 5 wt%, no clear granular structure could be observed but rather a blurred appearance was noticed (Fig. 10g). Aggregation was supposed to form at a high TPA ratio. It is assumed that pure granules were formed by the silk-only fibers, while hybrid granules with TPA were generated by the silk composite fibers. These two types of granules competed with each other and were highly affected by the TPA ratios.

In our earlier study,[21] two types of β-sheets were formed in the silk composite films with competition between TPA and silk fibroins, where strain-induced crystallization was involved. However, in this work, the mechanism of nucleus-dependent crystallization was proposed and discussed to interpret how TPA strengthened silk composite fibers. The molecular weight of TPA molecules was much lower than that of silk molecules. From the shear initially generated during fiber formation to poststretching and incubation during posttreatment, TPA molecules more easily formed the nucleus than silk molecules with a lower nucleating barrier. In this context, heterogeneous nucleation from TPA molecules outperformed homogeneous nucleation and became a favorable manner to induce more crystallization for the silk matrix. Therefore, in terms of nucleating behaviors, heterogeneous nucleation competed in 0.5 wt% TPA and was prominent in 1–3 wt% TPA but failed in excessive TPA of 5 wt%.

TPA exhibited distinct reinforcing mechanisms when it was introduced in different silk formats, like film and fiber. Even within the same silk format, the filler can behave in an opposite manner to affect the secondary structure of silk fibroins. As earlier reported,[48] carbon nanotubes (CNTs) could be used to reinforce the silk fibers by feeding them to silkworms. This additive hindered the crystallization of silk fibers with increased elongation at break and modulus. However, in another case,[42] CNTs were investigated to shorten the nucleation induction time of silk fibroin nanofibrils, and increase the content of β-crystallites/β-conformations in the composite fiber. Overall, the reinforcing mechanism depends on a variety of factors, such as the filler (*e.g.* type, content and shape), processing methods and silk formats.

Herein, a discussion is made to reveal the relationship between the nucleation behavior and mechanical properties of silk composite fibers. It is widely accepted that nucleation highly affects crystallization (such as crystallinity, crystallite size and orientation), which will straightforwardly determine the final mechanical properties. Increasing the force reeling speed for native spiders/silkworms[45,49] or conducting the poststretching of artificial silk fibers in air/alcohols[50] has been proven to be effective in improving the mechanical properties as a result of increased crystallinity/orientation but with decreased crystallite size. In this work, after the addition of TPA, there were no obvious changes in the peak positions and crystallite size for the silk-only and composite fibers. This implied that the crystal lattice of the silk matrix was not altered by heterogeneous nucleation. However, heterogeneous nucleation was favorably formed because of the low nucleating barrier, facilitating crystallization with an increase in crystallinity. Interestingly, 1 wt% was considered the most suitable concentration for TPA to reinforce the silk fibers with the highest crystallinity and good orientation. No significant difference in the mechanical properties was observed before and after the addition of 0.5 wt% TPA. Starting at 3 wt%, TPA aggregation partly formed and became very notable at 5 wt%, which led to the adverse mechanical performance with the lowest crystallinity and orientation.

Conclusions

In this work, TPA was synthesized as the dopant to reinforce silk composite fibers. At ratios from 0.5 to 5 wt%, TPA was mixed with silk fibroins using HFIP to form a miscible spinning dope, which mainly adopted a random coil structure. After wet spinning in an isopropanol solution, β-sheets were generated within pristine silk fibers, and their content gradually increased with increasing TPA ratio. After posttreatment, the β-sheet-rich structure of the resultant silk fibers was confirmed by both Raman and FTIR spectroscopy. Interestingly, the improved mechanical properties of silk composite fibers were demonstrated after the addition of TPA to silk fibroins, especially at ratios of 1 and 3 wt%. The best tensile strength of 250 MPa and toughness of 44 MJ m^{-3} were achieved for the Silk/TPA-1 and Silk/TPA-3 fibers, respectively, which were 42% and 51% higher than those of the silk-only fibers. As illustrated by WAXD, TPA could facilitate the crystallization of silk fibroins, and the highest crystallinity of 30% was obtained for the Silk/TPA-1 fiber, contributing to its impressive mechanical properties. Ultimately, a strengthening mechanism related to nucleus-dependent crystallization was discussed and further supported by simultaneous stretching during WAXD measurement, where TPA did not independently form crystallization. Interestingly, the higher-order stacking and alignment of granules observed by AFM may make a difference in the mechanical performance of silk composite fibers. This work elucidates the functionality of TPA as a dopant, describing its potential to extend to other biomaterial matrices for improved mechanical behavior.

Conflicts of interest

There are no conflicts to declare.

Acknowledgements

References

1 K. Numata, *Biopolymer Science for Proteins and Peptides*, Elsevier, 2021.

2 A. D. Malay, T. Suzuki, T. Katashima, N. Kono, K. Arakawa and K. Numata, *Sci. Adv.*, 2020, **6**, eabb6030.

3 Q. Wan, M. Yang, J. Hu, F. Lei, Y. Shuai, J. Wang, C. Holland, C. Rodenburg and M. Yang, *Nat. Commun.*, 2021, **12**, 1–8.

4 D. N. Rockwood, R. C. Preda, T. Yücel, X. Wang, M. L. Lovett and D. L. Kaplan, *Nat. Protoc.*, 2011, **6**, 1612–1631.

5 K. Spiess, A. Lammel and T. Scheibel, *Macromol. Biosci.*, 2010, **10**, 998–1007.

6 J. Chen, J. Hu, S. Sasaki and K. Naka, *ACS Biomater. Sci. Eng.*, 2018, **4**, 2748–2757.

7 N. A. Oktaviani, A. Matsugami, F. Hayashi and K. Numata, *Chem. Commun.*, 2019, **55**, 9761–9764.

8 T. Asakura, Y. Suzuki, Y. Nakazawa, G. P. Holland and J. L. Yarger, *Soft Matter*, 2013, **9**, 11440–11450.

9 G. P. Holland, M. S. Creager, J. E. Jenkins, R. V. Lewis and J. L. Yarger, *J. Am. Chem. Soc.*, 2008, **130**, 9871–9877.

10 A. D. Malay, R. Sato, K. Yazawa, H. Watanabe, N. Ifuku, H. Masunaga, T. Hikima, J. Guan, B. B. Mandal and S. Damrongsakkul, *Sci. Rep.*, 2016, **6**, 1–11.

11 G. Fang, S. Sapru, S. Behera, J. Yao, Z. Shao, S. C. Kundu and X. Chen, *J. Mater. Chem. B*, 2016, **4**, 4337–4347.

12 C. Guo, J. Zhang, J. S. Jordan, X. Wang, R. W. Henning and J. L. Yarger, *Biomacromolecules*, 2018, **19**, 906–917.

13 K. Numata, R. Sato, K. Yazawa, T. Hikima and H. Masunaga, *Polymer*, 2015, **77**, 87–94.

14 H. Sogawa, T. Korawit, H. Masunaga and K. Numata, *Molecules*, 2020, **25**, 235.

15 X.-L. Lin, L.-L. Gao, R.-x. Li, W. Cheng, C.-Q. Zhang and X.-z. Zhang, *Mater. Sci. Eng., C*, 2019, **105**, 110018.

16 X. Huang, S. Bai, Q. Lu, X. Liu, S. Liu and H. Zhu, *J. Biomed. Mater. Res., Part B*, 2015, **103**, 1402–1414.

17 P. Gupta, M. Adhikary, M. Kumar, N. Bhardwaj and B. B. Mandal, *ACS Appl. Mater. Interfaces*, 2016, **8**, 30797–30810.

18 H.-Y. Cheung, K.-T. Lau, Y.-F. Pow, Y.-Q. Zhao and D. Hui, *Composites, Part B*, 2010, **41**, 223–228.

19 Y. Zhao, J. Gong, C. Niu, Z. Wei, J. Shi, G. Li, Y. Yang and H. Wang, *J. Biomater. Sci., Polym. Ed.*, 2017, **28**, 2171–2185.

20 S. Zhao, X. Ye, M. Wu, J. Ruan, X. Wang, X. Tang and B. Zhong, *Int. J. Mol. Sci.*, 2021, **22**, 1513.

21 K. Tsuchiya, H. Masunaga and K. Numata, *Biomacromolecules*, 2017, **18**, 1002–1009.

22 K. Tsuchiya, T. Ishii, H. Masunaga and K. Numata, *Sci. Rep.*, 2018, **8**, 1–9.

23 J. Chen, Y. Ohta, H. Nakamura, H. Masunaga and K. Numata, *Polym. J.*, 2021, **53**, 179–189.

24 K. Tsuchiya and K. Numata, *Macromol. Biosci.*, 2017, **17**, 1700177.

25 P. J. Baker and K. Numata, *Biomacromolecules*, 2012, **13**, 947–951.

26 J. Fagerland, A. Finne-Wistrand and K. Numata, *Biomacromolecules*, 2014, **15**, 735–743.

27 A. P. Hammersley, *J. Appl. Crystallogr.*, 2016, **49**, 646–652.

28 L. F. Drummy, B. L. Farmer and R. R. Naik, *Soft Matter*, 2007, **3**, 877–882.

29 K. Tsuchiya and K. Numata, *Macromol. Biosci.*, 2016, **16**, 1001–1008.

30 S.-W. Ha, T. Asakura and R. Kishore, *Biomacromolecules*, 2006, **7**, 18–23.

31 K. A. Trabbic and P. Yager, *Macromolecules*, 1998, **31**, 462–471.

32 J. Chen, J. Hu, P. Zuo, J. Shi and M. Yang, *Int. J. Biol. Macromol.*, 2018, **116**, 1146–1152.

33 S. T. Krishnaji, G. Bratzel, M. E. Kinahan, J. A. Kluge, C. Staii, J. Y. Wong, M. J. Buehler and D. L. Kaplan, *Adv. Funct. Mater.*, 2013, **23**, 241–253.

34 M. Preghenella, G. Pezzotti and C. Migliaresi, *J. Raman Spectrosc.*, 2007, **38**, 522–536.

35 P. Monti, P. Taddei, G. Freddi, T. Asakura and M. Tsukada, *J. Raman Spectrosc.*, 2001, **32**, 103–107.

36 T. Lefèvre, M.-E. Rousseau and M. Pézolet, *Biophys. J.*, 2007, **92**, 2885–2895.

37 Y. Shen, M. A. Johnson and D. C. Martin, *Macromolecules*, 1998, **31**, 8857–8864.

38 S. Arnott, S. D. Dover and A. Elliott, *J. Mol. Biol.*, 1967, **30**, 201–208.

39 C. Fu, D. Porter, X. Chen, F. Vollrath and Z. Shao, *Adv. Funct. Mater.*, 2011, **21**, 729–737.

40 K. Yazawa, A. D. Malay, N. Ifuku, T. Ishii, H. Masunaga, T. Hikima and K. Numata, *Biomacromolecules*, 2018, **19**, 2227–2237.

41 X. Hu, D. Kaplan and P. Cebe, *Macromolecules*, 2006, **39**, 6161–6170.

42 L. Ma, Q. Liu, R. Wu, Z. Meng, A. Patil, R. Yu, Y. Yang, S. Zhu, X. Fan, C. Hou, Y. Li, W. Qiu, L. Huang, J. Wang, N. Lin, Y. Wan, J. Hu and X. Y. Liu, *Small*, 2020, **16**, 2000203.

43 K. Numata, H. Masunaga, T. Hikima, S. Sasaki, K. Sekiyama and M. Takata, *Soft Matter*, 2015, **11**, 6335–6342.

44 T. Seydel, K. Kölln, I. Krasnov, I. Diddens, N. Hauptmann, G. Helms, M. Ogurreck, S.-G. Kang, M. M. Koza and M. Müller, *Macromolecules*, 2007, **40**, 1035–1042.

45 N. Du, X. Y. Liu, J. Narayanan, L. Li, M. L. M. Lim and D. Li, *Biophys. J.*, 2006, **91**, 4528–4535.

46 T.-Y. Lin, H. Masunaga, R. Sato, A. D. Malay, K. Toyooka, T. Hikima and K. Numata, *Biomacromolecules*, 2017, **18**, 1350–1355.

47 S. Hofmann, C. W. P. Foo, F. Rossetti, M. Textor, G. Vunjak-Novakovic, D. L. Kaplan, H. P. Merkle and L. Meinel, *J. Controlled Release*, 2006, **111**, 219–227.

48 Q. Wang, C. Wang, M. Zhang, M. Jian and Y. Zhang, *Nano Lett.*, 2016, **16**, 6695–6700.

49 C. Riekel and F. Vollrath, *Int. J. Biol. Macromol.*, 2001, **29**, 203–210.

50 Q. Peng, Y. Zhang, L. Lu, H. Shao, K. Qin, X. Hu and X. Xia, *Sci. Rep.*, 2016, **6**, 36473.